Organic Electronics 39 (2016) 153–162

Contents lists available at ScienceDirect

Organic Electronics

journal homepage: www.elsevier.com/locate/orgel

Charge transport, doping and luminescence in solution-processed, phosphorescent, air-stable tellurophene thin films

Arash Mohammadpour [a, ****], Benjamin D. Wiltshire [a], Samira Farsinezhad [a], Yun Zhang [a], Abdelrahman M. Askar [a], Ryan Kisslinger [a], William T. Delgado [b], Gang He [b], Piyush Kar [a, ***], Eric Rivard [b, **], Karthik Shankar [a, c, *]

[a] Department of Electrical & Computer Engineering, University of Alberta, Edmonton, AB T6G 1H9, Canada
[b] Department of Chemistry, University of Alberta, Edmonton, AB T6G 2G2, Canada
[c] NRC National Institute for Nanotechnology, 11421 Saskatchewan Dr. NW, Edmonton, AB T6G 2M9, Canada

ARTICLE INFO

Article history:
Received 9 August 2016
Received in revised form
2 October 2016
Accepted 3 October 2016
Available online 7 October 2016

Keywords:
Inorganic heterocycles
Pi conjugated semiconductors
Metallacycle transfer
Field-effect
Raman spectra
Iodine intercalation

ABSTRACT

Recently synthesized small molecule tellurophenes containing ring-appended pinacolboronate (BPin) side groups possess remarkable guest-free air-stable solid-state phosphorescence, structure-based color-tunability and aggregation induced enhanced emission. The charge transport, doping and luminescence behavior of thin transparent films of a tellurophene with BPin groups positioned at the 2,5-positions (**B-Te-6-B**) was investigated. Film formation played a critical role in determining the hole mobility and the photoluminescence (PL) lifetime. Drop-coated films showed the strongest crystallinity, the highest PL quantum yields and a hole mobility (μ_p) of 1.1×10^{-4} cm^2 V^{-1} s^{-1}, which places tellurophenes in a select group of high mobility phosphorescent emitters. **B-Te-6-B** was also found to spontaneously form high aspect-ratio microwires upon drop-casting from supersaturated solutions. Oxidative doping in solution by a $N(C_6H_4Br)_3[SbCl_6]/LiNTf_2$ reagent combination ($Tf = SO_2CF_3$) increased conductivity by 2-4 orders of magnitude without inducing a color change in the films, while exposure to iodine vapor induced a dramatic change in color together with a 4-6 order of magnitude change in the conductivity. The optical transparency, facile electrical doping and relatively high hole mobilities of **B-Te-6-B** in solution processed thin films offer promise for the use of tellurophenes as host-free emissive layers and hole transport layers in organic optoelectronic devices.

1. Introduction

Oligothiophenes and polythiophenes are among the most widely studied organic semiconductors due to the combination of high absorption coefficients, good charge transport properties in solution-processed thin films and good performance in electronic devices such as organic field effect transistors and organic photovoltaics (OPV) [1–7]. Some drawbacks of solution processed neat films of oligothiophenes and polythiophenes include low luminescence quantum yields rendering them unacceptable as emissive layers in organic light emitting diodes (OLEDs), hole mobilities lower than acene-type organic semiconductors, and poor absorption of red and infrared photons (needed for high efficiency solar cells). With a view toward modifying and improving upon the optoelectronic properties of oligothiophenes – siloles, germoles and selenophenes have been synthesized and tested [8–11]. Π-conjugated organic small molecules containing one or more carbon atoms in the ring substituted by a heavier atom such as Si, Ge and Se have received significant attention in recent years due to the beneficial effects expected from the high polarizability of the heavy atom [12–17]. These effects include a higher dielectric constant (and refractive index) that follow directly from the Clausius-Mosotti equation as well as more red-shifted optical transitions. Substitution of the S atom in thiophenes with their heavier element congeners selenium and tellurium has also been found to result in a tripling of the value of

* Corresponding author. Department of Electrical & Computer Engineering, University of Alberta, Edmonton, AB T6G 1H9, Canada.
** Corresponding author.
*** Corresponding author.
**** Corresponding author.
E-mail addresses: pkar1@ualberta.ca (P. Kar), erivard@ualberta.ca (E. Rivard), kshankar@ualberta.ca (K. Shankar).

http://dx.doi.org/10.1016/j.orgel.2016.10.001
1566-1199/

the non-resonant electronic second hyperpolarizability (γ) compared to thiophene, which is of interest for non-linear optics [18]. A wider electronic band-width and improved carrier transport parameters are also expected due to the higher polarizability and the stronger electronic coupling resulting from intermolecular Te-Te interactions [19,20].

In 2014, our team reported on the bright room temperature phosphorescence from a tellurophene containing ring-appended pinacolboronate (BPin) side groups (**B-Te-6-B**; Fig. 1), and extended this in 2015 to a broader class of tellurophenes and benzotellurophenes with color-tunability of the emission [21,22]. The photoluminescence behavior in these compounds was rendered unusual by the observation of the still-rare aggregation-induced enhanced phosphorescence (AIEP) (a special case of aggregation-induced enhanced emission) [23–27], the high ambient stability of the observed phosphorescence emission to oxygen and the essential participation of the boron-based BPin groups in the emission process. The rarity of room temperature solid-state phosphorescent organic compounds [28,29] is underscored by the relatively few examples of organic compounds known to show this effect. The ambient-stability, solution-processability, solid-state phosphorescence and optical transparency of tellurophenes renders them particularly attractive for use as undoped, singlet-doped and triplet-doped phosphorescent matrix emitters in OLEDs [30], and as triplet exciton transporters in bulk heterojunction OPVs to overcome the exciton diffusion bottleneck [31–33]. We report herein on the film formation, charge transport behavior and dopability of the **B-Te-6-B** tellurophene.

2. Experimental section

B-Te-6-B was synthesized according to procedures reported elsewhere [34], while all other reagents were obtained from commercial sources and used as received. In this work, we examined three different processing schemes for preparing tellurophene thin films, namely, thermal evaporation, spin coating, and drop coating. Evaporation was performed in a PVD-75 system from Kurt J. Lesker equipped with 4 ceramic crucibles surrounded with tungsten filaments. Evaporation of **B-Te-6-B** started at 65 °C and thin film deposition was completed at 80 °C at a chamber pressure of 2.5×10^{-6} Torr. For both spin coating and drop coating, tetrahydrofuran (THF) (99.5%, Fisher Scientific) was used as the solvent to dissolve the **B-Te-6-B**. Different concentrations of tellurophene were tested ranging from 40 mg mL^{-1} to 72 mg mL^{-1} with a typical volume of 50 μL used for both spin-coating and drop-coating. Fluorine-doped tin oxide (FTO) coated glass slides with a conductivity of 8 Ω sq^{-1}, bare single crystal Si wafers and thermal oxide-coated heavily doped Si wafers were adopted as substrates for film formation and electrical studies. For some of the samples, a spin-coated and dehydrated film of Poly(3,4-ethylenedioxythiophene)-poly(styrenesulfonate) (PEDOT:PSS) (1.3 wt % dispersion in H_2O, conductive grade, Sigma Aldrich) was coated on the FTO substrates prior to tellurophene deposition. For both two-terminal and three-terminal electrical measurements, a back-gated field effect transistor configuration was employed using the tellurophene film as the active layer, thermally grown SiO_2 as the gate dielectric and n^{++}–Si as the gate electrode. The oxide thickness was 200 nm, the channel length was 50 μm and the channel width was

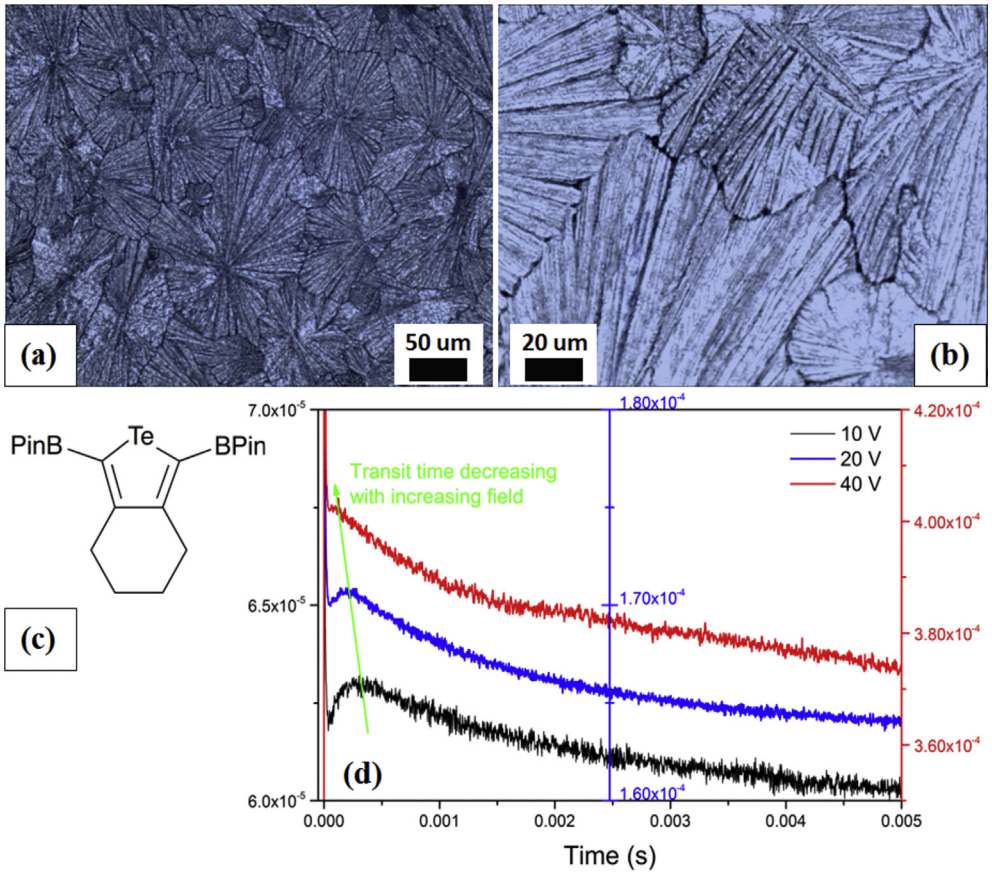

Fig. 1. Optical images for drop coated **B-Te-6-B** films (cast at 40 mg mL^{-1}) taken at magnifications of (a) 25× and (b) 50 ×; (c) shows the molecular structure of the **B-Te-6-B** tellurophene and (d) dark injection transients for drop coated **B-Te-6-B** films measured at three different voltages.

500 μm. For oxidative doping of the **B-Te-6-B** films, ~0.2% of $N(C_6H_4Br)_3[SbCl_6]$ (Across Organics, 95%) and 0.1–0.2 mM $Li(CF_3SO_2)_2N$ (Alfa Aesar, 98+%) were added to the drop-casting solution. Doping was also performed by exposing previously cast **B-Te-6-B** thin films either at room temperature or on a hot plate at 60 °C to iodine vapors in an air-tight jar for different periods of time ranging from 2 to 90 min. The vapor phase iodine exposure resulted in saturation at room temperature in about 75 min, while the saturation occurred at 60 °C in less than 10 min.

Tellurophene films prepared by the three schemes were characterized using different optical and electrical techniques. Steady-state photoluminescence (PL) spectra were collected using a Varian Cary Eclipse fluorescence spectrophotometer. A baseline sample of quartz was used to determine characteristic peaks for the **B-Te-6-B** films. The PL peak at ~550 nm was later analyzed using quantum yield (QY) measurements and lifetime measurements. Quantum yield measurements were performed using a Varian Cary Eclipse spectrofluorometer but with the use of fiber optic cables for illumination and the sample was held in an integrating sphere. The sample was illuminated with 337 nm light and the system gain was set to be as close as possible to saturating at 337 nm without actually reaching saturation. This allowed us to calculate the incident number of photons. Two tests were done per sample: one with the tellurophene sample in the path of the beam and the other with the sample removed from the path of the beam, but still in the integrating sphere. Similar background measurements with blank quartz were also done; as well as a scan with an empty integrating sphere. The results were then combined together with self-absorption and waveguiding corrections to find the quantum yield of the sample using the methods explained in Monkman et al. [35] and Garbuzov et al. [36]. Lifetime measurements were performed with a VSL337 nitrogen laser from Spectra-Physics whose output consisted of 337 nm pulses 3.5 ns in duration at a frequency of 20 Hz. We illuminated the sample with the N_2 laser, making sure any direct reflections would be blocked and not measured by our system. The PL decays were collected using a high speed photomultiplier tube (PMT) coupled to a high speed oscilloscope. The transient response at 530 nm was best fit to a dual-exponential curve and the two time constants were extracted. Optical images were acquired using ZEISS AX10 Lab microscope with different magnifications ranging from 2.5× to 50×. Raman spectra were collected with a Nicolet Almega XR Raman Spectrometer. Excitation was produced by a 532 nm laser operating at a power of 24 mW. An Olympus 10× objective with a numerical aperture of 0.25 and a 100 μm pinhole aperture were used, and the spot size was 2.1 μm. For dark injection measurements, application of the voltage step and recording of the dark injection transients were performed using a Keithley 4200 semiconductor parameter analyzer equipped with a Model 4225 ultra-fast pulse measurement unit (PMU). The rise time of the voltage step used was as small as 70 ns.

3. Results and discussion

3.1. Effect of film formation technique on charge transport, absorption and luminescence

Fig. 1(a) and (b) are optical micrographs for **B-Te-6-B** thin films drop cast from 40 mg mL^{-1} solutions in THF which show strikingly good crystallinity with large monocrystalline domains, which is quite rare, since the vast majority of phosphorescent materials and their films are amorphous [37–39]. Even when crystallinity is present, polycrystalline films of small molecule organic semiconductors typically consist of grain sizes in the tens of nanometers or sub-micron range [40–43]. The exceptions are high performance thin films of linear acene-type small molecules where grain sizes >1 mm are now routinely obtained [44–46]. The Van der Waals interactions involved in generating the morphology and crystallinity of organic semiconductor films are extremely sensitive to molecular structure and casting methods, due to which robust methods to manipulate the crystalline packing of π-conjugated small molecules for optimal electronic properties, are much needed [47]. In this context, the ability of tellurophenes to spontaneously form millimeter-sized grains in drop-cast thin films without recourse to confined crystallization, controlled deposition, anti-solvent methods or solution shearing, is quite significant [48,49]. Closer examination of the grain boundaries (*cf.* Fig. 1(b)) indicates a number of low angle grain boundaries and even some where the alignment extends across grains, suggestive of longer range ordering. It is well-documented that high crystallinity, longer range ordering and low angle grain boundaries are strongly correlated with superior charge and energy transport in thin films of π-conjugated small molecules [50,51]. Furthermore polytellurophenes have been reported to have field effect hole mobilities of 10^{-4}–10^{-3} cm^2V^{-1} s^{-1} [52]. Therefore, we examined charge transport in **B-Te-6-B** films using time-resolved dark injection (TR-DI) measurements, which allowed us to both deduce the ohmicity of the contact and measure the carrier mobility [53].

TR-DI (schematic illustration provided in Fig. S1 in Supporting Information) involves measurement of the transient current in response to a voltage step and has significant advantages compared to the competing Time-of-Flight (TOF) technique for mobility measurement for thin organic films wherein there exists the need for a film thickness much larger than the penetration depth of the laser light and the transit time in dispersive materials is not easily discernible [54]. In TR-DI, a characteristic peak is observed at a time $\boldsymbol{t_{DI}}$ due to space charge limited carrier transport (SCLC), from which the carrier mobility ($\boldsymbol{\mu_p}$) may be extracted from its expression [55], $\boldsymbol{\mu_p} = 0.786\boldsymbol{L^2}/\boldsymbol{t_{DI}V}$, where $\boldsymbol{L}$ is the film thickness and $\boldsymbol{V}$ is the magnitude of the applied voltage step. The results of the TR-DI measurements are shown in Fig. 1(d). Since a positive voltage step was applied at the FTO/PEDOT:PSS contact, hole injection is implied. *p*-type conduction in the **B-Te-6-B** films was also verified in three-terminal measurements by modulating the channel conduction between bottom contacted source-drain electrodes using a back-gated electrode (See Supporting Information Fig. S2). While conduction is suppressed at positive values of gate bias and almost entirely suppressed at $\boldsymbol{V_{GS}} = 100$ V, conduction in the channel is dramatically enhanced at negative values of gate bias, which is indicative of preferential hole conduction in the **B-Te-6-B** thin films (Supporting Information Figs. S2a and S2b). Despite clear modulation of channel conduction by gate bias, the observed three-terminal electrical behavior falls short of field-effect transistor (FET) behavior since the I_D–V_{DS} curves neither show a clear threshold voltage nor exhibit saturation for high values of drain bias, which we attribute to strong trapping and space charge effects in the films. From the expression for $\boldsymbol{\mu_p}$, the hole mobility was calculated to be 1.1×10^{-4} cm^2V^{-1} s^{-1} for drop-coated **B-Te-6-B** thin films. The contact injection efficiency is given by the ratio of the transient current in Fig. 1(d) to the space charge limited current that exists at longer time durations, and was found to exceed 90% indicating an ohmic contact with the FTO electrode. Electron transport was measured using TR-DI by application of a negative pulse at the FTO contact. Even though this measurement is non-ideal due to the non-ohmicity of the contact for electron injection, it was still possible to probe electron transport in drop-coated **B-Te-6-B** films because the contact injection efficiency and trapping phenomena exercise only a limited influence on the value of the measured mobility [56]. These measurements (Supporting Information Fig. S11) show that a precise peak in the SCLC transient is not easy to determine since the current response plateaus after

roughly 10 ms, due to which the transit time is difficult to estimate reliably. Such behavior is characteristic of highly dispersive electron transport and μ_n was estimated to lie in the range 10^{-6} – 10^{-8} cm^2 V^{-1} s^{-1}.

There is a concerted move in the OLED field to move to non-doped devices based on emissive phosphorescent neat films (self-host design) in order to mitigate interlayer mixing, to overcome phase segregation in the doped layer, to lower drive voltages by eliminating guest molecule-induced deep carrier traps, to avoid the need for very wide bandgap hosts for blue emission and to improve electron injection by avoiding host materials with shallow LUMOs [57,58]. However, the host-free non-doped device strategy requires good carrier mobilities in neat films of the emissive phosphor, which has been substantially difficult to achieve. For neat films of bis(2-phenylpyridinato-*N*,$C^{2'}$)iridium(acetylacetonate) ($(ppy)_2Ir$(acac)) which is a phosphorescent green emitter used as both host and guest in PHOLEDs, Tsuzuki and Tokito determined a relatively high hole mobility of 2.4×10^{-5} cm^2V^{-1} s^{-1} compared to *fac*-tris(2-phenylpyridinato-*N*,$C^{2'}$)iridium ($Ir(ppy)_3$) neat films wherein both electron and hole transport were found to be too dispersive to reliably estimate a mobility [59]. Subsequently, Peng et al. reported a mobility of ~10^{-3} cm^2 V^{-1} s^{-1} for both electrons and holes in neat films of the phosphorescent host green emitter [bis(4,6-di-fluorophenyl)pyridinato-*N*,$C^{2'}$]iridium(*N*,*N*′-diisopropylbenzamidine) ($(Fppy)_2Ir$(dipba)) [60]. In this context, our observation of a hole mobility of ~10^{-4} cm^2 V^{-1} s^{-1} in neat films of a small molecule tellurophene with an unoptimized molecular structure, is quite remarkable and points to the excellent potential of tellurophenes for usage in organic electronic devices.

Fig. 2 shows the results of TR-DI measurements in evaporated and spin-coated thin films. In the inset of Fig. 2(a), the optical micrograph at 10× magnification suggests islands of **B-Te-6-B** on the substrate, but the evaporated film is actually continuous as seen in the 50× optical micrograph in the inset of Fig. 2(a), also confirmed by cross-sectional SEM imaging (Supporting Information Fig. S10). The apparent islands are merely regions of the film containing larger grains and taller features. Estimates of the film thickness using ellipsometry (Supporting Information Fig. S7). and backed up by a quartz crystal monitor for evaporated films (~80 nm), were more reliable than thickness measurements by cross-sectional field-emission SEM. This is because the low sublimation temperature (~65 °C) in high vacuum (~1 mTorr) of the **B-Te-6-B** films rendered them susceptible to thickness reduction due to sublimation during chamber loading and imaging in ultrahigh vacuum. Using ellipsometry, the spin-coated films were estimated to have a thickness of 205 nm (Supporting Information Fig. S8). By extracting the characteristic times for dark injection in Fig. 2(a) and (b), and using them in the expression of μ_p (as mentioned previously), we obtained a hole mobility of 5.1×10^{-7} cm^2 V^{-1} s^{-1} for the evaporated film and 7.9×10^{-10} cm^2 V^{-1} s^{-1} for the spin-coated film. We thus observe by comparison with the results shown in Fig. 1(d) that charge transport deteriorates by several orders of magnitude as the film formation method is varied from the large crystalline grain-forming drop-casting technique to thermal evaporation and spin-coating. Spin-coating is a rapid and highly non-equilibrium process that does not lend itself to the growth of crystals, and therefore results in films with the poorest charge transport. The correlation between film morphology and opto-electronic properties extends to photoluminescence quantum yields and lifetimes as shown in Table 1. Graphs of the time-resolved PL as well as detailed fitting data are provided in the Supporting Information Figs. S3–S5. Drop-coated films have the highest PL quantum yields approaching 12% and also exhibit significantly longer lifetimes than spin-coated films for both of the long-lived components in bi-exponential decays, which we attribute to enhanced crystallinity in the drop-coated films that restricts intramolecular rotation and suppresses vibrational non-radiative relaxation pathways. Evaporated films present a slightly curious case, wherein the charge transport and PL quantum yield are inferior to drop-coated films but the lifetime components are longer. The origin of this behavior is unclear to us at this time. Further increases in the PL quantum yield will be enabled if the molecular structure is modified such that rotation of the boron-containing sidegroups is suppressed. A more rigid emitter with the boronate esters locked in place would reduce non-radiative decay pathways for excited states.

Thin film samples of drop-coated, spin-coated and thermally-evaporated **B-Te-6-B** were also prepared on transparent fluorine-doped tin oxide (FTO)-coated glass substrates. The optical absorption spectra and steady-state PL spectra of drop-coated, spin coated and thermally evaporated films of **B-Te-6-B** are shown in Fig. 3 while the corresponding excitation spectra are shown in Supporting Information Fig. S6. Thermally-evaporated film samples were studied using regular transmittance mode. However, because of the translucency of drop-coated film samples, their optical absorption was measured using an integrating sphere. As shown in Fig. 3(a), the drop-coated films exhibit an absorption edge at ~380 nm, red-shifted by nearly 10 nm from the corresponding absorption edge in spin-coated films due to a larger conjugation length in the highly crystalline drop-coated films

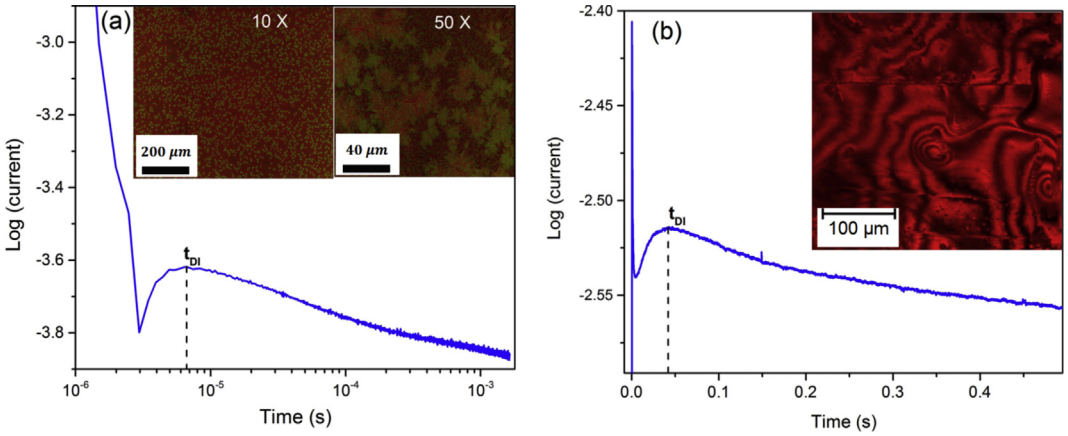

Fig. 2. Dark injection transients for (a) evaporated and (b) spin-coated **B-Te-6-B** thin films. The insets in (a) and (b) correspond to optical micrographs of the respective film morphologies.

Table 1
PL quantum yields, lifetimes, and goodness of fit data for drop-coated, spin-coated and thermally evaporated tellurophene films.

	PL quantum yield	Lifetimes (μs)	Goodness-of-fit (Adj. R-square)
Drop-Coated	11.5%	$t_1 = 95.87$, $t_2 = 18.31$	99.858%
Thermally-evaporated	3.4%	$t_1 = 118.83$, $t_2 = 23.66$	99.553%
Spin-Coated	1.7%	$t_1 = 78.66$, $t_2 = 10.76$	90.818%

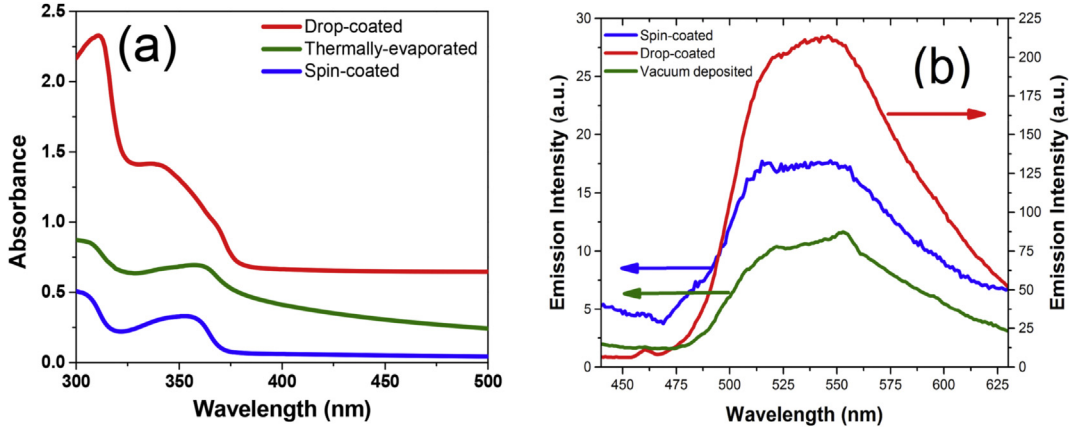

Fig. 3. (a) Absorption spectra and (b) PL spectra of drop-coated (40 mg/mL), spin-coated (40 mg/mL), and thermally-evaporated tellurophene films.

(also confirmed in Supporting Information Fig. S6a). The drop-coated films also display a richer vibronic structure with peaks at *ca.* 310 nm, 340 nm and 370 nm as seen in Fig. 3(a). The evaporated films show a very strong Urbach tail [61,62] of sub-bandgap states extending to 500 nm, which is indicative of a large amount of disorder in the films. For PL measurement, thin films were deposited on a quartz substrate in order to minimize the interference of the substrate luminescence. The PL spectra in Fig. 3(b) under 350 nm excitation show that undoped drop-coated **B-Te-6-B** films have a strong emission peak at ~560 nm. The same emission peak is present in evaporated **B-Te-6-B** films, albeit weaker and blue-shifted. It is worth mentioning here that this tellurophene (and related BPin-functionalized analogues) show an amazing ambient stability of phosphorescent emission. For example, two different tellurophene films of **B-Te-6-B** prepared nearly one year apart, have identical luminescence spectra (not shown here). The sensitivity of the phosphorescence lifetimes to the type of packing present may allow mechanical force-induced luminescence sensing using tellurophene compounds [63].

3.2. Spontaneous formation of microwires

An intriguing observation in this study is the spontaneous formation of microwires following drop-casting from saturated solutions of **B-Te-6-B** in THF (72 mg mL^{-1}) as demonstrated in Fig. 4. Such a spontaneous formation of microwires has also been observed for other crystalline small molecule organic semiconductors such as Alq_3 [64,65], diaminoanthraquinone [66], perylene derivatives [67], etc. The density of formation of microwires was found to be a strong function of the type of substrate used. Fig. 4(c) shows microwires fusing to form a continuous film. Sparse microwires were formed on clean Si surfaces (Fig. 4(a) and (c)) while an extremely dense nucleation of **B-Te-6-B** microwires was observed on FTO and SiO_2 surfaces (Fig. 4(b), (c), 4(e) and 4(f)), which in turn could point to a relationship between surface energy and microwire nucleation.

3.3. Doping of B-Te-6-B films

We also examined chemical doping of **B-Te-6-B** films to modulate their conductivity. Two different doping strategies were examined. The first involved using oxidative doping by $N(C_6H_4Br)_3[SbCl_6]$ with a small amount of lithium bis(trifluoromethanesulfonyl)imide, $LiNTf_2$ ($Tf = SO_2CF_3$) introduced into the solution from which the films were cast. This is a technique that has been effectively used to increase the conductivity of small molecule hole transporting organic semiconductors such as *N, N′*-diphenyl-*N, N′*-bis (3-methylphenyl)-1, 1′-biphenyl-4, 4′-diamine (TPD) and 2,2′,7,7′-tetrakis[*N*,*N*-di(4-methoxyphenyl)amino]-9,9′-pirobifluorene (spiro-OMeTAD) as well as to dope polymers such as polythiophenes, polypyrrole, polyisoprene and polyacetylene to render them conductive [68–71]. The particular recipes used by us leaned heavily on the ones used in previous reports to dope small molecule hole transporters in high efficiency solid-state solar cells [72–74]. The *I-V* characteristics (red curve in Fig. 5(a)) showed a two- to four-order magnitude increase in the conductivity of drop-coated $N(C_6H_4Br)_3[SbCl_6]$-doped **B-Te-6-B** films. The UV–Vis spectrum of $N(C_6H_4Br)_3[SbCl_6]$-doped **B-Te-6-B** films (Supporting Information Fig. S12) is similar to that of the undoped films at short wavelengths with an absorption edge at ~385 nm, but then manifests a different behavior for longer wavelengths (>500 nm) in the form of a steadily increasing absorption, which is characteristic of the behavior of free carriers. Furthermore, the films do not exhibit a perceptible change in the macroscopic color of the drop-cast films. On the other hand, exposure to iodine vapors (second doping strategy) for even a few minutes at room temperature produces a dramatic change in color from transparent with a yellowish tinge for undoped films as seen in Fig. 5(c)—a deep orange in Fig. 5(d). Longer duration exposure to I_2 for 20 min at high temperatures results in a further change in color to deep red (green under a dark background) as seen in Fig. 5(e). In the following text and figures, heavy I_2 doping is used to refer to conditions that result in intensely colored films while moderate doping produces less intense color. **B-Te-6-B** films were heavily doped with I_2 by exposing them to I_2 vapor for 15 min at 110 °C. These changes in color are seen as

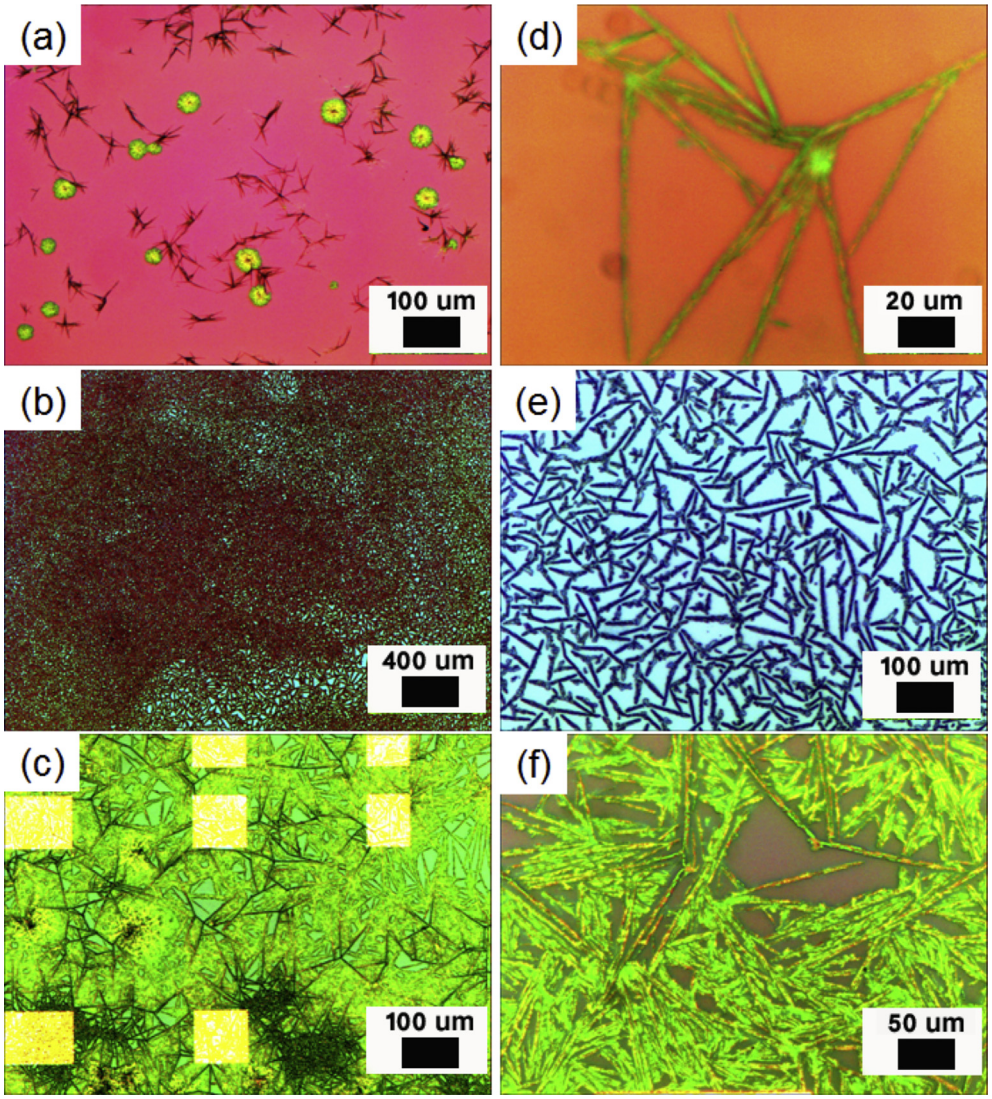

Fig. 4. Optical micrographs of tellurophene microwires formed by drop-casting from supersaturated **B-Te-6-B** solutions (72–75 mg mL^{-1}) on to various substrates, (a), (b) and (c) correspond to bare Si, FTO:glass and patterned SiO_2/Si substrates respectively while (d), (e) and (f) present the corresponding images at higher magnification.

intense new absorption bands in the UV–Vis spectra and are also accompanied by dramatic changes in the electrical conductivity (blue curve in Fig. 5(a)), which increases by four-to-six orders of magnitude over that of the undoped films. Visually, the drop-coated film sample became strongly reddish (green under a dark background) when iodine doped whereas thermally-evaporated film samples did not show a visible color change. A small increment in the absorption of the thermally-evaporated sample after I_2 doping might be an indication of poor doping.

Iodine doping of thiophene oligomers results in a two-three order change in the electrical conductivity and an increase in optical absorption. I_2 doping completely quenches the luminescence of doped **B-Te-6-B** samples (Supporting Information Fig. S6b). Iodine doping of organic semiconductors can occur due to one of the following three phenomena (which can co-exist and also overlap): (i) Intercalation of iodine atoms into the π-stack between molecular layers, as occurs in pentacene [75] together with the formation of charge transfer complexes due to interaction between weakly donating conjugated molecules and iodine acceptors as occurs in single walled carbon nanotubes [76] and graphene [77] (ii) Radical ion salt formation due to massive charge transfer and (iii) *p*-doping due to iodine acting as an oxidizing agent as occurs in trans-polyacetylene and other conjugated polymers [78]. In Supporting Information Fig. S12, the signature long wavelength absorption of free carriers is observed for $N(C_6H_4Br)_3[SbCl_6]$-doped films but not for iodine doped ones (Fig. 5(b)), allowing us to discount possibility (iii). A direct chemical reaction between iodine and **B-Te-6-B** was ruled on the basis of NMR analysis of products of reacting iodine with **B-Te-6-B** for 24 h in toluene at room temperature (Supporting Information Figs. S13–S16). Closer inspection of the optical spectra (Fig. 5(b)) of moderately doped and saturation doped **B-Te-6-B** films reveals strongly increased absorption between 440 nm and 500 nm, presumably due to the absorption of molecular iodine [79]. However, the absorption of the I_2-doped films extends to 700 nm while the absorption of ultraviolet photons with wavelengths <400 nm, is also strongly enhanced. Such behavior is typically due to the formation of charged polyiodide species, as is evidenced by the presence of triiodide (I_3^-) and pentaiodide (I_5^-) species in the Raman spectra of the iodine doped B-Te-6-B (reported below), and is also further backed up by the observation of high conductivity in saturation I_2 doped **B-Te-6-B** films in Fig. 5(a) [80–82].

Iodine doping of thiophene oligomers (n = 2–5) resulted in a three-four order of magnitude increase in the conductivity along

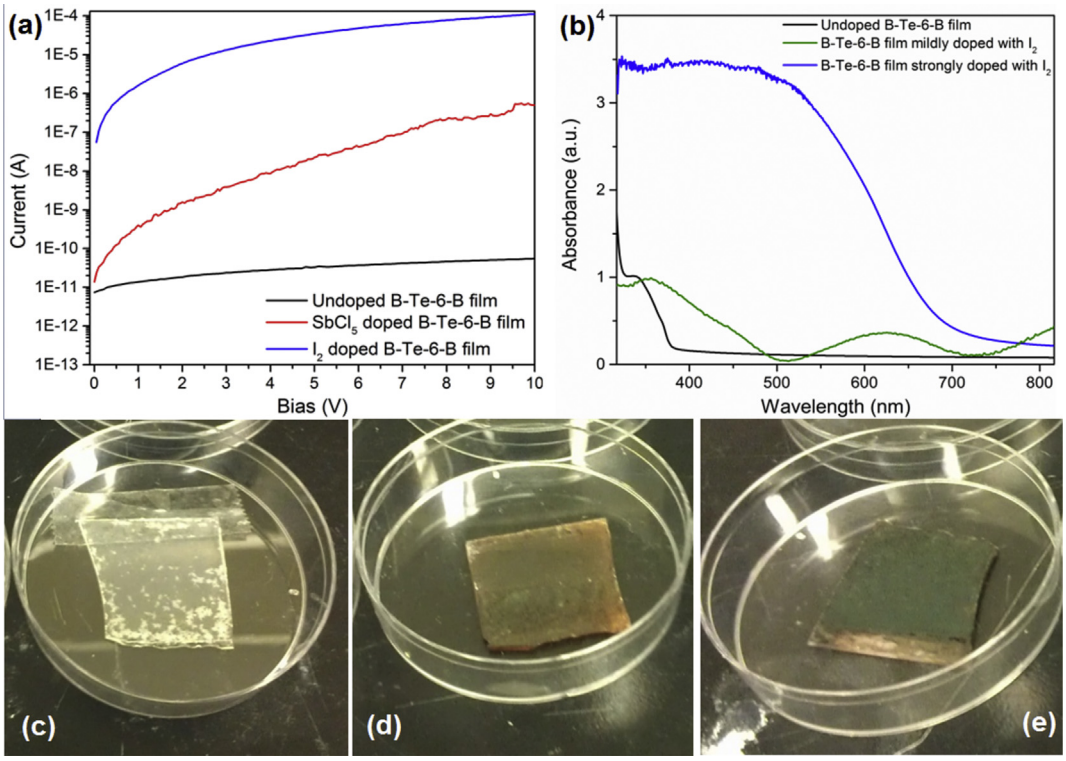

Fig. 5. Effect of $SbCl_5$ solution doping and iodine vapor doping on the (a) Electrical conductivity (b) Optical spectra and (c), (d) and (e) Macroscopic sample color of drop-coated **B-Te-6-B** films. Please see the experimental section and the text for details related to the method and duration of the doping treatments. (For interpretation of the references to colour in this figure legend, the reader is referred to the web version of this article.)

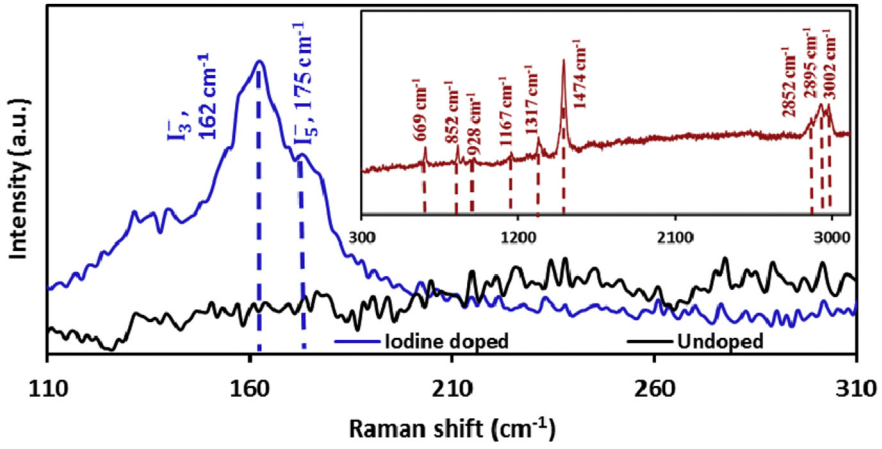

Fig. 6. Raman spectra for iodine doped and undoped **B-Te-6-B**. Inset shows Raman spectra for the undoped **B-Te-6-B** in the in the 300 to 3000 cm^{-1} frequency window illustrating the tellurophene specific peaks.

with an absorption peak in the visible [80,83]. Oligoselenophenes (n = 2–5) showed a conductivity of 10^{-5}-10^{-3} S cm^{-1} following vapor phase iodine doping [77]. The higher conductivities were obtained for a larger number of repeat units and the conductivity values were similar to those obtained for doped oligothiophenes [84]. Therefore, the conductivity of ~0.001 S cm^{-1} obtained for an iodine-doped tellurophene monomer in this study (Fig. 5(a)) compares favorably with prior studies.

3.4. Raman spectra of B-Te-6-B films

Raman spectra for iodine doped and undoped **B-Te-6-B** films formed by drop-coating were obtained to analyze the presence of charged polyiodide species, and are shown in Fig. 6. In the 100 cm^{-1}–300 cm^{-1} frequency window, the iodine doped **B-Te-6-B** exhibits distinct peaks at 162 cm^{-1} and 175 cm^{-1}. We attribute intercalated charged triiodide (I_3^-) species to the peak at 162 cm^{-1} [85–87] and charged pentaiodide (I_5^-) species to the peak at 175 cm^{-1} [82,88]. Higher frequency Raman spectrum for **B-Te-6-B**, shown in the inset, exhibits tellurophene-specific peaks; these may be assigned to out-of-plane C-H deformation at 669 cm^{-1}, out-of-plane C-H bend at 852 cm^{-1} and 928 cm^{-1}, in-plane C-H deformation at 1167 cm^{-1}, ring stretch at 1474 cm^{-1}, and C-H stretches at 2852 cm^{-1}, 2895 cm^{-1}, and 3002 cm^{-1} [89–92].

4. Conclusion

Recently synthesized small molecule tellurophenes have shown

remarkable luminescence properties such as air-stable phosphorescent emission, structure-tunable emission color and aggregation induced enhanced phosphorescence. However their charge transport properties have remained unknown. In this report, we studied charge transport and doping in solution processed thin films of the small molecule tellurophene **B-Te-6-B**. We found that the process of film formation plays a critical role in determining the optoelectronic properties of the resulting **B-Te-6-B** films. While all films were found to be *p*-type, drop-coated films showed the highest hole mobility of 1.1×10^{-4} cm^2 V^{-1} s^{-1} while the hole mobilities of the thermally evaporated and spin-coated films were found to be orders of magnitude lower. Likewise, drop-coated films also had the highest PL quantum yields and PL lifetimes longer than that of spin-coated films. Such a strong film formation dependency of the optoelectronic properties was related to crystallinity as drop-coated films were found to be the most crystalline of the three types of films with a morphology that consisted of large crystalline grains with low angle boundaries. Drop-casting from supersaturated solutions of **B-Te-6-B** in THF was also found to result in the spontaneous formation of high aspect ratio microwires. Two different types of chemical doping strategies were studied. Doping by $N(C_6H_4Br)_3[SbCl_6]/LiNTf_2$ reagent combination was found to have relatively no effect on the color and optical absorption of the films while increasing film conductivity by 2-4 orders of magnitude. Doping by exposure to iodine vapors resulted in dramatic changes in color and optical absorption accompanied by a 4-6 order of magnitude increase in the electrical conductivity of the **B-Te-6-B** films. On the basis of Raman spectra, the presence of intercalated I_3^- and I_5^- is confirmed, which is a likely cause for the enhancement of electrical conductivity. In addition to their potential use as phosphorescent emissive layers in sensors and light emitting devices, the present work shows that undoped small molecule tellurophenes have a comparable or higher hole mobility than spiro-OMeTAD (~10^{-4} cm^2 V^{-1} s^{-1}) [93], and could therefore function as transparent hole transporters in OPVs and OLEDs. Furthermore, the molecular structure of **B-Te-6-B** is not optimized for charge transport. Optimization of molecular design might result in further increases in charge carrier mobility rendering them relevant to a broader range of electronic applications.

Acknowledgements

All authors thank NSERC (385970) for funding support (Discovery and CREATE grants). Some device fabrication and testing used research infrastructure made possible by a Leaders Opportunity Fund grants to K.S. and E.R. from the Canada Foundation for Innovation (CFI) (24661) and the Alberta Small Equipment Grants Program (SEGP) (URSI-10-032-SEG). Measurement of some photoluminescence lifetimes by Lorenz Mayr is acknowledged. A.M., S.F. and B.D.W. acknowledge scholarship support from Alberta Innovates - Technology Futures (AITF), while E.R. thanks AITF for a New Faculty Award.

Appendix A. Supplementary data

Supplementary data related to this article can be found at http://dx.doi.org/10.1016/j.orgel.2016.10.001.

References

[1] A. Mishra, C.Q. Ma, P. Bauerle, Functional oligothiophenes: molecular design for multidimensional nanoarchitectures and their applications, Chem. Rev. 109 (2009) 1141–1276.
[2] Y.K. Lan, C.H. Yang, H.C. Yang, Theoretical investigations of electronic structure and charge transport properties in polythiophene-based organic field-effect transistors, Polym. Int. 59 (2010) 16–21.
[3] M.L. Capobianco, G. Barbarella, A. Manetto, Oligothiophenes as fluorescent markers for biological applications, Molecules 17 (2012) 910–933.
[4] C.B. Nielsen, I. McCulloch, Recent advances in transistor performance of polythiophenes, Prog. Polym. Sci. 38 (2013) 2053–2069.
[5] H.J. Wang, C.P. Chen, R.J. Jeng, Polythiophenes comprising conjugated pendants for polymer solar cells: a review, Materials 7 (2014) 2411–2439.
[6] L. Zhang, N.S. Colella, B.P. Cherniawski, S.C.B. Mannsfeld, A.L. Briseno, Oligothiophene semiconductors: synthesis, characterization, and applications for organic devices, ACS Appl. Mater. Interfaces 6 (2014) 5327–5343.
[7] L. Guan, X.Y. Zhang, F.Q. Sun, Y. Jiang, Y.P. Zhong, P. Liu, Oligothiophene derivatives in organic photovoltaic devices, Prog. Chem. 27 (2015) 1435–1447.
[8] S.J. Toal, H. Sohn, L.N. Zakarov, W.S. Kassel, J.A. Golen, A.L. Rheingold, W.C. Trogler, Syntheses of oligometalloles by catalytic dehydrocoupling, Organometallics 24 (2005) 3081–3087.
[9] S.J. Toal, D. Magde, W.C. Trogler, Luminescent oligo(tetraphenyl)silole nanoparticles as chemical sensors for aqueous TNT, Chem. Commun. (2005) 5465–5467.
[10] Y. Kunugi, K. Takimiya, K. Yamane, K. Yamashita, Y. Aso, T. Otsubo, Organic field-effect transistor Using oligoselenophene as an active layer, Chem. Mater 15 (2003) 6–7.
[11] K.A. Mazzio, M. Yuan, K. Okamoto, C.K. Luscombe, Oligoselenophene derivatives functionalized with a diketopyrrolopyrrole core for molecular bulk heterojunction solar cells, ACS Appl. Mater. Interfaces 3 (2011) 271–278.
[12] J.W. Chen, Y. Cao, Silole-containing polymers: chemistry and optoelectronic properties, Macromol. Rapid Commun. 28 (2007) 1714–1742.
[13] G. Lu, H. Usta, C. Risko, L. Wang, A. Facchetti, M.A. Ratner, T.J. Marks, Synthesis, characterization, and transistor response of semiconducting silole polymers with substantial hole mobility and air stability. Experiment and theory, J. Am. Chem. Soc. 130 (2008) 7670–7685.
[14] D. Gendron, P.O. Morin, P. Berrouard, N. Allard, B.R. Aich, C.N. Garon, Y. Tao, M. Leclerc, Synthesis and photovoltaic properties of poly(dithieno 3,2-b:2′,3′-d germole) derivatives, Macromolecules 44 (2011) 7188–7193.
[15] J. Hollinger, D. Gao, D.S. Seferos, Selenophene electronics, Isr. J. Chem. 54 (2014) 440–453.
[16] S.H. Roh, H. Cheong, J. Park, H. Sohn, M.S. Cho, H.G. Woo, Synthesis and characterization of phosphine/borane-terminated poly(silole-co-germole) for the evaluation of luminescent polymer light-emitting diode, J. Nanosci. Nanotechnol. 14 (2014) 6438–6441.
[17] S.M. Parke, M.P. Boone, E. Rivard, Marriage of heavy main group elements with π-conjugated materials for optoelectronic applications, Chem. Commun. 52 (2016) 9485–9505.
[18] K. Kamada, T. Sugino, M. Ueda, K. Tawa, Y. Shimizu, K. Ohta, Femtosecond optical Kerr study of heavy-atom effects on the third-order optical nonlinearity of thiophene homologues: electronic hyperpolarizability of tellurophene, Chem. Phys. Lett. 302 (1999) 615–620.
[19] E.I. Carrera, D.S. Seferos, Semiconducting polymers containing tellurium: perspectives toward obtaining high-performance materials, Macromolecules 48 (2015) 297–308.
[20] E. Rivard, Tellurophenes and their emergence as building blocks for polymeric and light-emitting materials, Chem. Lett. 44 (2015) 730–736.
[21] G. He, W. Torres Delgado, D.J. Schatz, C. Merten, A. Mohammadpour, L. Mayr, M.J. Ferguson, R. McDonald, A. Brown, K. Shankar, E. Rivard, Coaxing solid-state phosphorescence from tellurophenes, Angew. Chem. Int. Ed. 53 (2014) 4587–4591.
[22] G. He, B.D. Wiltshire, P. Choi, A. Savin, S. Sun, A. Mohammadpour, M.J. Ferguson, R. McDonald, S. Farsinezhad, A. Brown, K. Shankar, E. Rivard, Phosphorescence within benzotellurophenes and color tunable tellurophenes under ambient conditions, Chem. Commun. 51 (2015) 5444–5447.
[23] Q. Zhao, L. Li, F. Li, M. Yu, Z. Liu, T. Yi, C. Huang, Aggregation-induced phosphorescent emission (AIPE) of iridium(iii) complexes, Chem. Commun. (2008) 685–687.
[24] O. Toma, N. Mercier, M. Allain, A. Forni, F. Meinardi, C. Botta, Aggregation induced phosphorescent N-oxyde-2,2[prime or minute]-bipyridine bismuth complexes and polymorphism-dependent emission, Dalton Trans. 44 (2015) 14589–14593.
[25] J. Mei, N.L. Leung, R.T. Kwok, J.W. Lam, B.Z. Tang, Aggregation-induced emission: together we shine, united we soar!, Chem. Rev. 115 (2015) 11718–11940.
[26] Y. Hong, J.W.Y. Lam, B.Z. Tang, Aggregation-induced emission: phenomenon, mechanism and applications, Chem. Commun. (2009) 4332–4353.
[27] J. Mei, Y. Hong, J.W.Y. Lam, A. Qin, Y. Tang, B.Z. Tang, Aggregation-induced emission: the whole Is more brilliant than the parts, Adv. Mater. 26 (2014) 5429–5479.
[28] S. Mukherjee, P. Thilagar, Recent advances in purely organic phosphorescent materials, Chem. Commun. 51 (2015) 10988–11003.
[29] W.Z. Yuan, X.Y. Shen, H. Zhao, J.W.Y. Lam, L. Tang, P. Lu, C. Wang, Y. Liu, Z. Wang, Q. Zheng, J.Z. Sun, Y. Ma, B.Z. Tang, Crystallization-induced phosphorescence of pure organic luminogens at room temperature, J. Phys. Chem. C 114 (2010) 6090–6099.
[30] H. Uoyama, K. Goushi, K. Shizu, H. Nomura, C. Adachi, Highly efficient organic light-emitting diodes from delayed fluorescence, Nature 492 (2012) 234–238.
[31] N.C. Giebink, Y. Sun, S.R. Forrest, Transient analysis of triplet exciton dynamics in amorphous organic semiconductor thin films, Org. Electron 7 (2006) 375–386.
[32] I. Kim, H.M. Haverinen, Z. Wang, S. Madakuni, Y. Kim, J. Li, G.E. Jabbour,

Efficient organic solar cells based on planar metallophthalocyanines, Chem. Mater. 21 (2009) 4256–4260.
[33] S.M. Menke, R.J. Holmes, Exciton diffusion in organic photovoltaic cells, Energy Environ. Sci. 7 (2014) 499–512.
[34] G. He, L. Kang, W. Torres Delgado, O. Shynkaruk, M.J. Ferguson, R. McDonald, E. Rivard, The marriage of metallacycle transfer chemistry with Suzuki–Miyaura cross-coupling to give main group element-containing conjugated polymers, J. Am. Chem. Soc. 135 (2013) 5360–5363.
[35] L.-O. Pålsson, A.P. Monkman, Measurements of solid-state photoluminescence quantum yields of films using a fluorimeter, Adv. Mater. 14 (2002) 757.
[36] D.Z. Garbuzov, V. Bulović, P.E. Burrows, S.R. Forrest, Photoluminescence efficiency and absorption of aluminum-tris-quinolate (Alq3) thin films, Chem. Phys. Lett. 249 (1996) 433–437.
[37] B. D'Andrade, S.R. Forrest, Formation of triplet excimers and dimers in amorphous organic thin films and light emitting devices, Chem. Phys. 286 (2003) 321–335.
[38] J.C. Ostrowski, M.R. Robinson, A.J. Heeger, G.C. Bazan, Amorphous iridium complexes for electrophosphorescent light emitting devices, Chem. Commun. (2002) 784–785.
[39] G. Zhou, W.-Y. Wong, B. Yao, Z. Xie, L. Wang, Triphenylamine-dendronized pure red iridium phosphors with superior OLED efficiency/color purity tradeoffs, Angew. Chem. Int. Ed. 46 (2007) 1149–1151.
[40] Z. Pan, N. Rawat, I. Cour, L. Manning, R.L. Headrick, M. Furis, Polarization-resolved spectroscopy imaging of grain boundaries and optical excitations in crystalline organic thin films, Nat. Commun. 6 (2015) 8201.
[41] J. Rivnay, S.C. Mannsfeld, C.E. Miller, A. Salleo, M.F. Toney, Quantitative determination of organic semiconductor microstructure from the molecular to device scale, Chem. Rev. 112 (2012) 5488–5519.
[42] F. Zhang, C.A. Di, N. Berdunov, Y. Hu, Y. Hu, X. Gao, Q. Meng, H. Sirringhaus, D. Zhu, Ultrathin film organic transistors: precise control of semiconductor thickness via spin-coating, Adv. Mater. 25 (2013) 1401–1407.
[43] G. Horowitz, M.E. Hajlaoui, Mobility in polycrystalline oligothiophene field-effect transistors dependent on grain size, Adv. Mater. 12 (2000) 1046–1050.
[44] R.L. Headrick, S. Wo, F. Sansoz, J.E. Anthony, Anisotropic mobility in large grain size solution processed organic semiconductor thin films, Appl. Phys. Lett. 92 (2008) 063302.
[45] Y. Diao, B.C.K. Tee, G. Giri, J. Xu, D.H. Kim, H.A. Becerril, R.M. Stoltenberg, T.H. Lee, G. Xue, S.C.B. Mannsfeld, Z. Bao, Solution coating of large-area organic semiconductor thin films with aligned single-crystalline domains, Nat. Mater. 12 (2013) 665–671.
[46] K.C. Dickey, J.E. Anthony, Y.L. Loo, Improving organic thin-film transistor performance through solvent-vapor annealing of solution-processable triethylsilylethynyl anthradithiophene, Adv. Mater. 18 (2006) 1721–1726.
[47] J. Wan, Y. Li, J.G. Ulbrandt, D.-M. Smilgies, J. Hollin, A.C. Whalley, R.L. Headrick, Transient phases during fast crystallization of organic thin films from solution, APL Mater 4 (2016) 016103.
[48] L. Shaw, Z.N. Bao, The large-area, solution-based deposition of single-crystal organic semiconductors, Isr. J. Chem. 54 (2014) 496–512.
[49] A.M. Hiszpanski, Y.-L. Loo, Directing the film structure of organic semiconductors via post-deposition processing for transistor and solar cell applications, Energy Environ. Sci. 7 (2014) 592–608.
[50] J. Rivnay, L.H. Jimison, J.E. Northrup, M.F. Toney, R. Noriega, S. Lu, T.J. Marks, A. Facchetti, A. Salleo, Large modulation of carrier transport by grain-boundary molecular packing and microstructure in organic thin films, Nat. Mater 8 (2009) 952–958.
[51] Y. Diao, L. Shaw, Z.A. Bao, S.C.B. Mannsfeld, Morphology control strategies for solution-processed organic semiconductor thin films, Energy Environ. Sci. 7 (2014) 2145–2159.
[52] A.A. Jahnke, L. Yu, N. Coombs, A.D. Scaccabarozzi, A.J. Tilley, P.M. DiCarmine, A. Amassian, N. Stingelin, D.S. Seferos, Polytellurophenes provide imaging contrast towards unravelling the structure–property–function relationships in semiconductor: insulator polymer blends, J. Mater. Chem. C 3 (2015) 3767–3773.
[53] B.K. Yap, S.P. Koh, S.K. Tiong, C.N. Ong, Space-charge-limited dark injection (SCL DI) transient measurements, Semiconductor Electronics (ICSE), in: 2010 IEEE International Conference, 2010, pp. 192–194.
[54] D. Poplavskyy, J. Nelson, D.D.C. Bradley, Ohmic hole injection in poly(9,9-dioctylfluorene) polymer light-emitting diodes, Appl. Phys. Lett. 83 (2003) 707–709.
[55] A. Many, G. Rakavy, Theory of transient space-charge-limited currents in solids in the presence of trapping, Phys. Rev. 126 (1962) 1980–1988.
[56] M.Z. Szymanski, I. Kulszewicz-Bajer, J. Faure-Vincent, D. Djurado, Transport properties of triarylamine based dendrimers studied by space charge limited current transients, Opt. Mater 34 (2012) 1630–1634.
[57] J. Ding, B. Wang, Z. Yue, B. Yao, Z. Xie, Y. Cheng, L. Wang, X. Jing, F. Wang, Bifunctional green iridium dendrimers with a “Self-Host” feature for highly efficient nondoped electrophosphorescent devices, Angew. Chem. Int. Ed. 48 (2009) 6664–6666.
[58] L. Chen, Z. Ma, J. Ding, L. Wang, X. Jing, F. Wang, Effect of dendron generation on properties of self-host heteroleptic green light-emitting iridium dendrimers, Org. Electron 13 (2012) 2160–2166.
[59] T. Tsuzuki, S. Tokito, Highly efficient and low-voltage phosphorescent organic light-emitting diodes using an iridium complex as the host material, Adv. Mater 19 (2007) 276–280.
[60] T. Peng, Y. Yang, Y. Liu, D. Ma, Z. Hou, Y. Wang, A phosphorescent material with high and balanced carrier mobility for efficient OLEDs, Chem. Commun. 47 (2011) 3150–3152.
[61] A.E. Rakhshani, Study of Urbach tail, bandgap energy and grain-boundary characteristics in CdS by modulated photocurrent spectroscopy, J. Phys. Condens. Matter 12 (2000) 4391.
[62] W.J.D. Beenken, F. Herrmann, M. Presselt, H. Hoppe, S. Shokhovets, G. Gobsch, E. Runge, Sub-bandgap absorption in organic solar cells: experiment and theory, Phys. Chem. Chem. Phys. 15 (2013) 16494–16502.
[63] P. Xue, J. Sun, P. Chen, P. Wang, B. Yao, P. Gong, Z. Zhang, R. Lu, Luminescence switching of a persistent room-temperature phosphorescent pure organic molecule in response to external stimuli, Chem. Commun. 51 (2015) 10381–10384.
[64] J. Boulet, A. Mohammadpour, K. Shankar, Insights into the solution crystallization of oriented Alq3 and Znq2 microprisms and nanorods, J. Nanosci. Nanotechnol. 15 (2015) 6680–6689.
[65] G. Xu, Y.-B. Tang, C.-H. Tsang, J.-A. Zapien, C.-S. Lee, N.-B. Wong, Facile solution synthesis without surfactant assistant for ultra long Alq3 sub-microwires and their enhanced field emission and waveguide properties, J. Mater. Chem. 20 (2010) 3006–3010.
[66] J.Y. Zheng, Y. Yan, X. Wang, Y.S. Zhao, J. Huang, J. Yao, Wire-on-Wire growth of fluorescent organic heterojunctions, J. Am. Chem. Soc. 134 (2012) 2880–2883.
[67] A.L. Briseno, S.C. Mannsfeld, C. Reese, J.M. Hancock, Y. Xiong, S.A. Jenekhe, Z. Bao, Y. Xia, Perylenediimide nanowires and their use in fabricating field-effect transistors and complementary inverters, Nano Lett. 7 (2007) 2847–2853.
[68] C. Ganzorig, K. Suga, M. Fujihira, p-type semiconductors of aromatic diamines doped with SbCl5, Chem. Lett. (2000) 1032–1033.
[69] S. Najidha, N. Saxena, R. Sreeja, C. Unnithan, P. Predeep, Optical and electrical characterization of SbCl 5 doped cis-1, 4-polyisoprene, Mater. Lett. 59 (2005) 3431–3436.
[70] L. Soderholm, C. Mathis, B. Francois, J. Friedt, The preparation, characterization and physical properties of SbCl5-doped polyacetylene, Synth. Met. 10 (1985) 261–272.
[71] I. Watanabe, M.F. Rubner, Doping studies of heterogeneous langmuir—-blodgett thin films containing poly(3-hexyl thiophene), Brit. Polym. J. 23 (1990) 165–170.
[72] L. Schmidt-Mende, J.E. Kroeze, J.R. Durrant, M.K. Nazeeruddin, M. Grätzel, Effect of hydrocarbon chain length of amphiphilic ruthenium dyes on solid-state dye-sensitized photovoltaics, Nano Lett. 5 (2005) 1315–1320.
[73] J.E. Kroeze, N. Hirata, S. Koops, M.K. Nazeeruddin, L. Schmidt-Mende, M. Grätzel, J.R. Durrant, Alkyl chain barriers for kinetic optimization in dye-sensitized solar cells, J. Am. Chem. Soc. 128 (2006) 16376–16383.
[74] M.J. Carnie, C. Charbonneau, M.L. Davies, J. Troughton, T.M. Watson, K. Wojciechowski, H. Snaith, D.A. Worsley, A one-step low temperature processing route for organolead halide perovskite solar cells, Chem. Commun. 49 (2013) 7893–7895.
[75] Y. Matsuo, A. Sasaki, Y. Yoshida, S. Ikehata, New stage structure of iodine doped pentacene film (II), Mol. Cryst. Liq. Crys. A 340 (2000) 223–228.
[76] J. Chen, M.A. Hamon, H. Hu, Y. Chen, A.M. Rao, P.C. Eklund, R.C. Haddon, Solution properties of single-walled carbon nanotubes, Science 282 (1998) 95–98.
[77] N. Jung, N. Kim, S. Jockusch, N.J. Turro, P. Kim, L. Brus, Charge transfer chemical doping of few layer graphenes: charge distribution and band gap formation, Nano Lett. 9 (2009) 4133–4137.
[78] H. Borchert, Physics and Chemistry of Conductive Polymers, Solar Cells Based on Colloidal Nanocrystals, Springer International Publishing, 2014, pp. 39–60.
[79] H. Goto, A possibility for construction of an iodine cleaning system based on doping for π-conjugated polymers, Polymers 3 (2011) 875–885.
[80] Y. Cao, D. Guo, M. Pang, R. Qian, Studies on iodine doped thiophene oligomers, Synth. Met. 18 (1987) 189–194.
[81] M. Brinkmann, V.S. Videva, A. Bieber, J.J. André, P. Turek, L. Zuppiroli, P. Bugnon, M. Schaer, F. Nuesch, R. Humphry-Baker, Electronic and structural evidences for charge transfer and localization in iodine-doped pentacene, J. Phys. Chem. A 108 (2004) 8170–8179.
[82] U. Venkateswaran, E. Brandsen, M. Katakowski, A. Harutyunyan, G. Chen, A. Loper, P. Eklund, Pressure dependence of the Raman modes in iodine-doped single-walled carbon nanotube bundles, Phys. Rev. B 65 (2002) 054102.
[83] S. Hotta, K. Waragai, Alkyl-substituted oligothiophenes: crystallographic and spectroscopic studies of neutral and doped forms, J. Mater. Chem. 1 (1991) 835–842.
[84] H. Nakanishi, S. Inoue, T. Otsubo, The first oligoselenophenes: synthesis and properties, Mol. Cryst. Liq. Crys. A 296 (1997) 335–348.
[85] E. Mulazzi, I. Pollini, L. Piseri, R. Tubino, Selective resonant Raman enhancement in polyiodide chains, Phys. Rev. B 24 (1981) 3555.
[86] A. Bandrauk, K. Truong, C. Carlone, S. Jandl, Resonance Raman spectrum of the I− 3 ion and the phase transition in the organic metal TMAITCNQ, Chem. Phys. Lett. 95 (1983) 78–82.
[87] R. Swietlik, D. Schweitzer, H.J. Keller, Resonance Raman investigations of the symmetric stretching mode of I3-anions in α and β phases of di-bis (ethylenedithio) tetrathiafulvalene tri-iodide, Phys. Rev. B 36 (1987) 6881.
[88] L. Grigorian, K. Williams, S. Fang, G. Sumanasekera, A. Loper, E. Dickey, S. Pennycook, P. Eklund, Reversible intercalation of charged iodine chains into carbon nanotube ropes, Phys. Rev. Lett. 80 (1998) 5560.
[89] G. Paliani, R. Cataliotti, A. Poletti, F. Fringuelli, A. Taticchi, M. Giorgini, Vibrational analysis of tellurophene and its deuterated derivatives, Spectrochim.

Acta A 32 (1976) 1089–1104.
[90] M.G. Giorgini, G. Paliani, R. Cataliotti, Vibrational spectra and assignments for tetrahydrothiophene, tetrahydroselenophene and tetrahydrotellurophene, Spectrochim. Acta A 33 (1977) 1083–1089.
[91] G. Paliani, R. Cataliotti, Vibrational spectra and assignments for 2-chloro and 2-bromo derivatives of thiophene, selenophene and tellurophene, Spectrochim. Acta A 37 (1981) 707–710.
[92] J.O. Jensen, Vibrational frequencies and structural determination of tellurophene, J. Mol. Struc. Theochem. 718 (2005) 209–218.
[93] D. Poplavskyy, J. Nelson, Nondispersive hole transport in amorphous films of methoxy-spirofluorene-arylamine organic compound, J. Appl. Phys. 93 (2003) 341–346.

Supporting Information

Charge Transport, Doping and Luminescence in Solution-Processed, Phosphorescent, Air-Stable Tellurophene Thin Films

Arash Mohammadpour,[a,] Benjamin D. Wiltshire,[a] Samira Farsinezhad,[a] Yun Zhang,[a] Abdelrahman M. Askar,[a] Ryan Kisslinger,[a] William T. Delgado,[b] Gang He,[b] Piyush Kar,[a,*] Eric Rivard,[b,*] and Karthik Shankar[a,c,]**

Author affiliations:

[a]Department of Electrical & Computer Engineering, University of Alberta, Edmonton, AB T6G 1H9, Canada

[b]Department of Chemistry, University of Alberta, Edmonton, AB T6G 2G2, Canada

[c] NRC National Institute for Nanotechnology, 11421 Saskatchewan Dr. NW, Edmonton, AB T6G 2M9

*** Authors to whom all correspondence must addressed:**

Prof. Karthik Shankar, email: kshankar@ualberta.ca

Prof. E. Rivard, email: erivard@ualberta.ca

Dr. Piyush Kar, email: pkar1@ualberta.ca

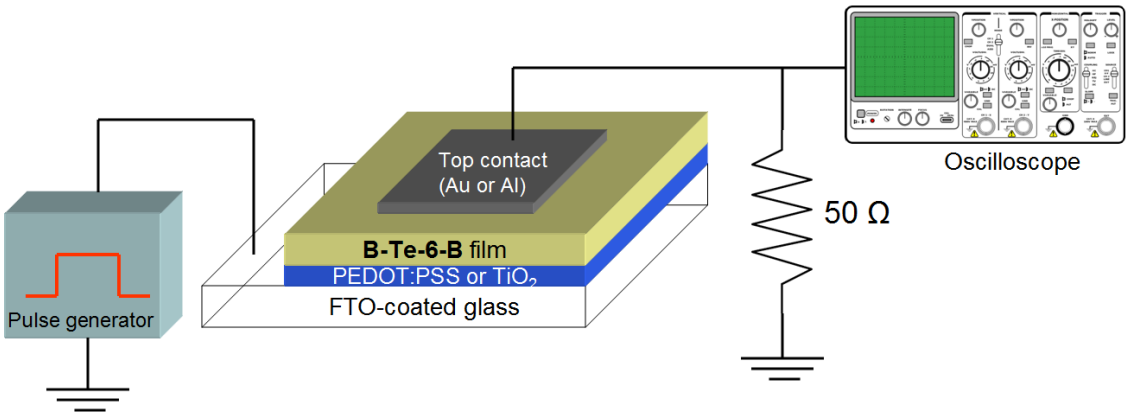

Figure S1: Schematic of the measurement setup for time-resolved dark injection. We acknowledge use of the oscilloscope image from jjbeard [Public domain], via Wikimedia Commons. In our set-up, a Keithley 4200 semiconductor parameter analyzer equipped with two ultrafast 4225 PMUs, was used to perform both the pulse generation and scope functions.

SI. Three-terminal electrical measurements of **B-Te-6-B** films

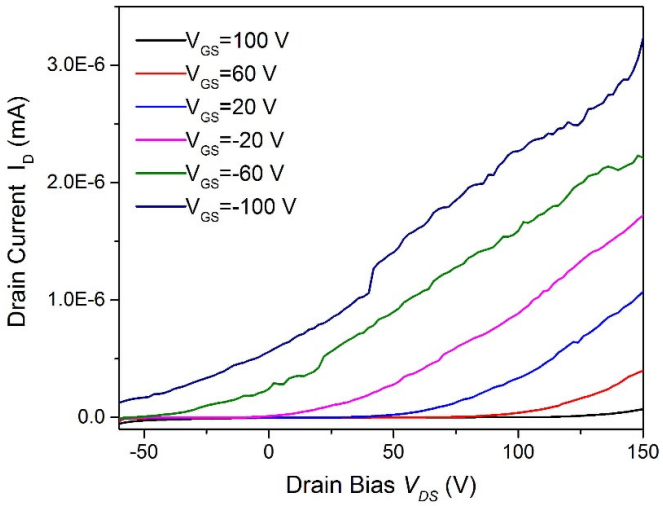

Figure S2a: Drain current vs. drain-source bias curves for different values of gate bias (V_{GS}).

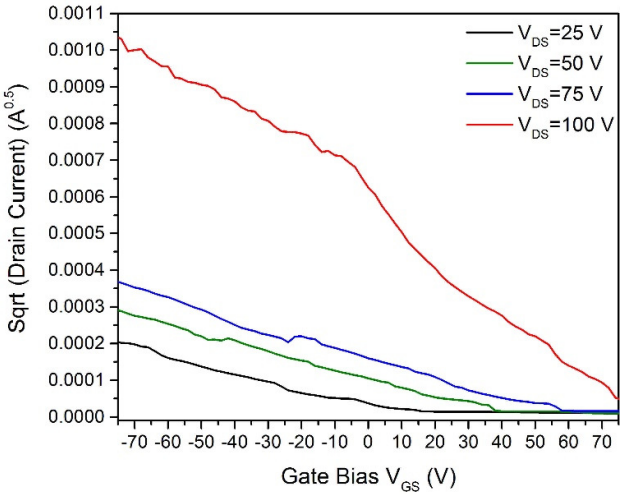

Figure S2b: Plots of the square root of the drain current versus gate bias curves for different values of drain source bias (V_{DS}).

SII. Time-resolved PL

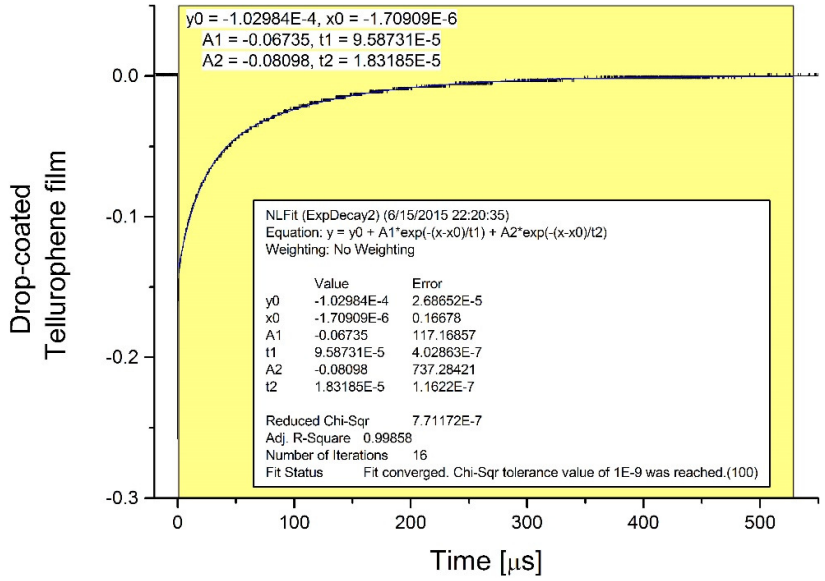

Figure S3: Measured time-resolved photoluminescence of drop-coated B-Te-6-B thin films along with biexponential fits to the observed decay. The table in the inset shows the fit parameters including the goodness of the fit.

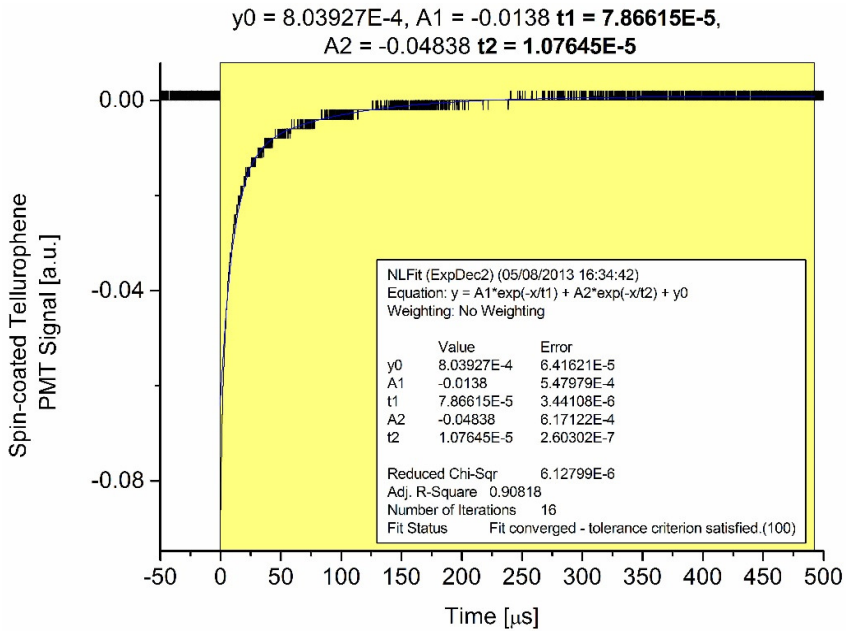

Figure S4: Measured time-resolved photoluminescence of spin-coated B-Te-6-B thin films along with biexponential fits to the observed decay. The table in the inset shows the fit parameters including the goodness of the fit.

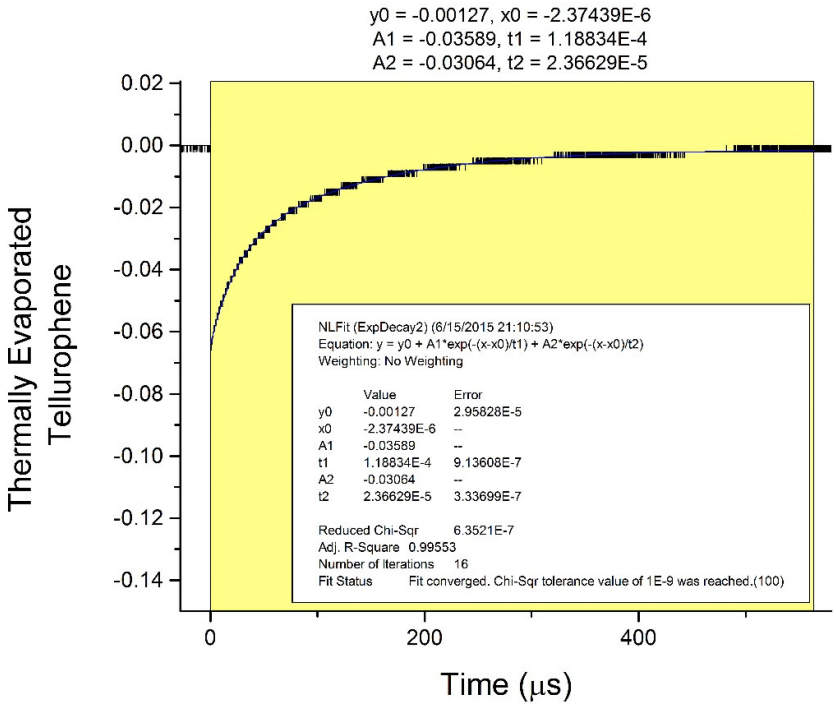

Figure S5: Measured time-resolved photoluminescence of thermally evaporated B-Te-6-B thin films along with biexponential fits to the observed decay. The table in the inset shows the fit parameters including the goodness of the fit.

SIII. Excitation Spectra of **B-Te-6-B** films

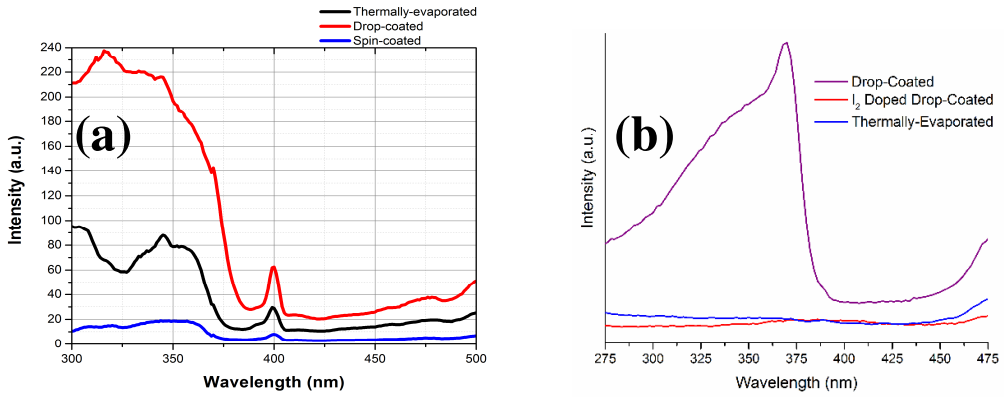

Figure S6: Measured excitation spectra of (a) drop-coated (red curve), spin-coated (blue curve) and thermally evaporated (black curve) and (b) drop-coated (purple curve), I_2 doped drop-coated (red curve) and thermally evaporated (black curve) thin films of **B-Te-6-B**. The PL emissions were monitored at 547 nm and 500 nm in (a) and (b) respectively.

SIV. Ellipsometry of **B-Te-6-B** thin films

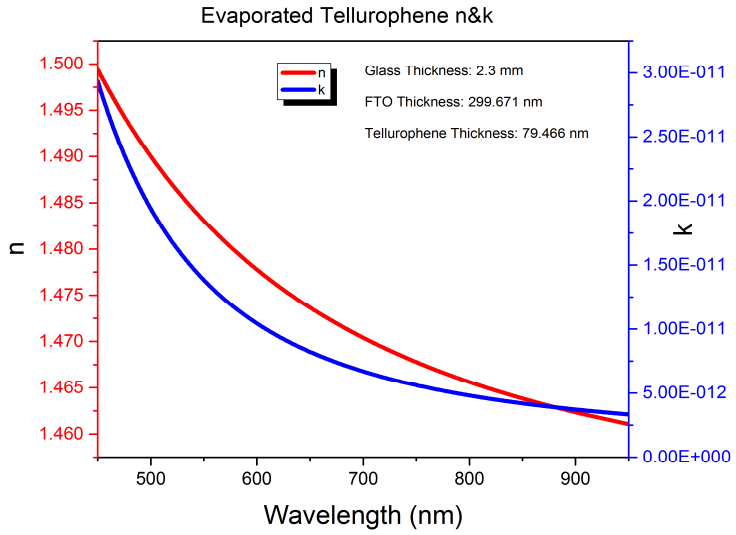

Figure S7: Extracted refractive index (*n*), extinction coefficient (*k*) and thickness (79.5 nm) of thermally evaporated B-Te-6-B thin films by fitting ellipsometric data to a multi-layer model incorporating surface roughness and void fraction while assuming the tellurophene film to exhibit Cauchy dispersion.

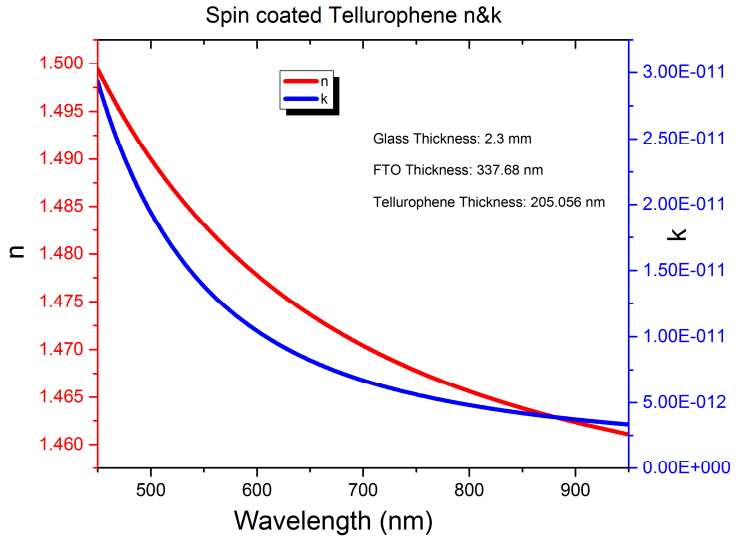

Figure S8: Extracted refractive index (*n*), extinction coefficient (*k*) and thickness (205.1 nm) of spin-coated B-Te-6-B thin films by fitting ellipsometric data to a multi-layer model incorporating surface roughness and void fraction while assuming the tellurophene film to exhibit Cauchy dispersion.

SV. Cross-sectional FESEM images of **B-Te-6-B** films

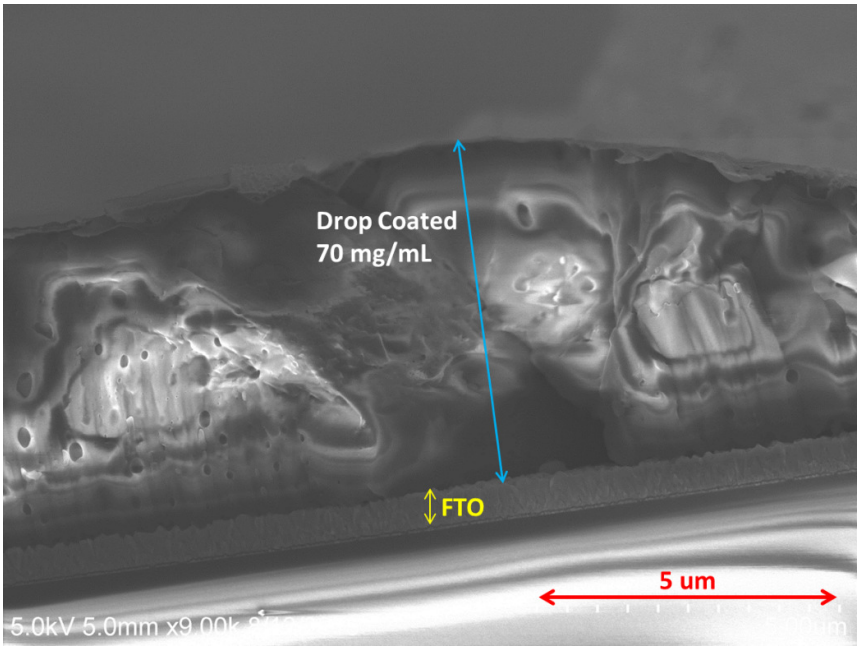

Figure S9: Field emission scanning electron microscope (FESEM) image of the cross-section of a **B-Te-6-B** film drop-coated on to a FTO-coated glass substrate.

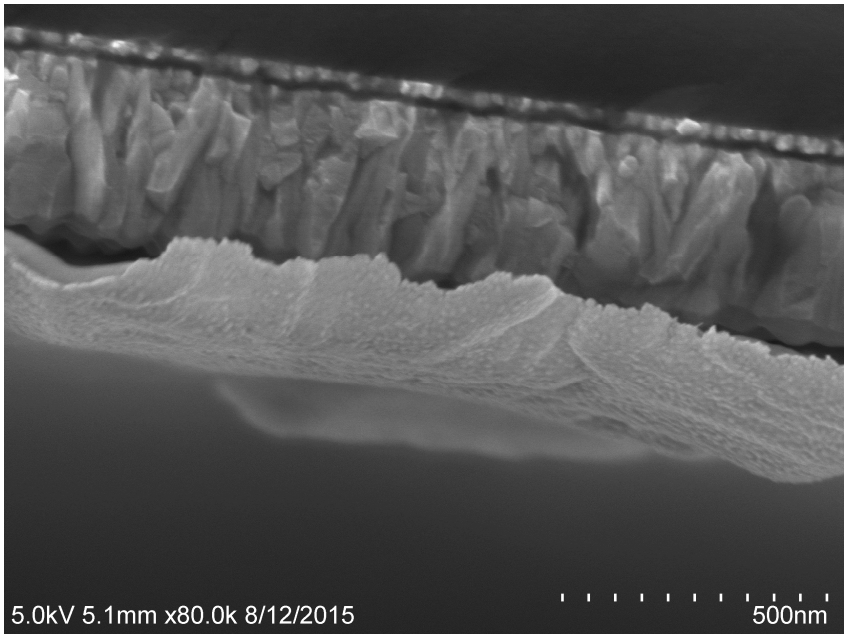

Figure S10: Field emission scanning electron microscope (FESEM) image of the cross-section of a **B-Te-6-B** film thermally evaporated on to a FTO-coated glass substrate.

SVI. Electron transport measurements in tellurophene films

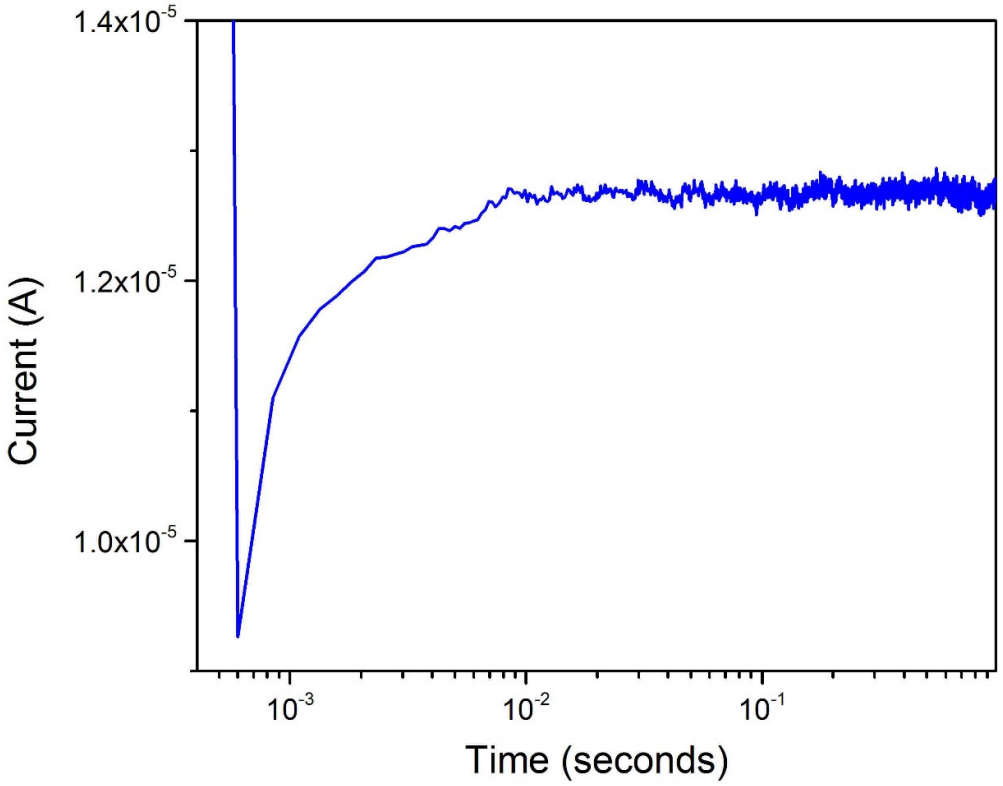

Figure S11: Dark injection transient for a drop coated **B-Te-6-B** film measured by the application of a –40 V pulse at the FTO electrode.

SVII. Additional UV-Vis spectra showing the effect of doping of **B-Te-6-B** films

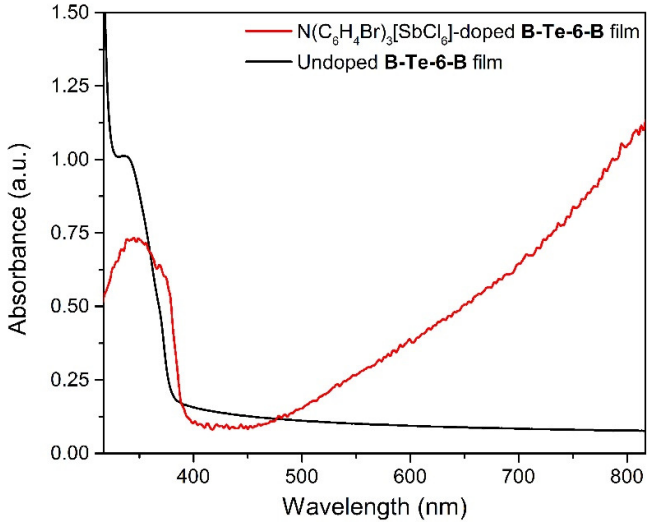

Figure S12: UV-vis spectra of drop-coated **B-Te-6-B** films showing the effect of oxidative doping by $N(C_6H_4Br)_3[SbCl_6]$/$LiNTf_2$.

SVIII. Solution phase reaction of **B-Te-6-B** with I_2

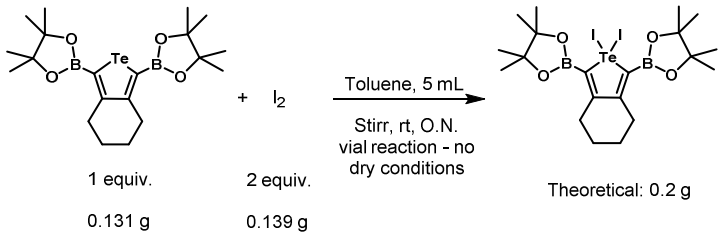

Figure S13: Reaction between iodine and **B-Te-6-B** in toluene at room temperature.

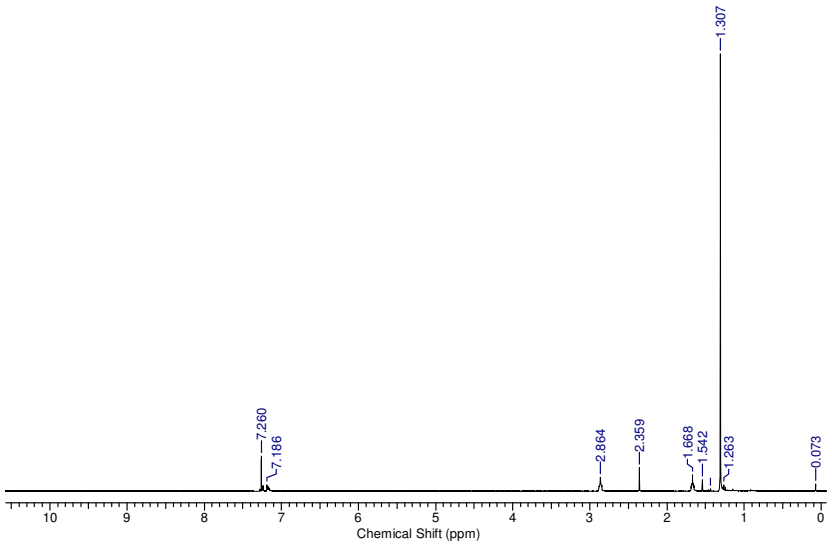

Figure S14: ^{1}H NMR spectrum of the reaction mixture in $CDCl_3$ upon removal of the volatiles; spectra data is consistent with no reaction between I_2 and **B-6-Te-B**.

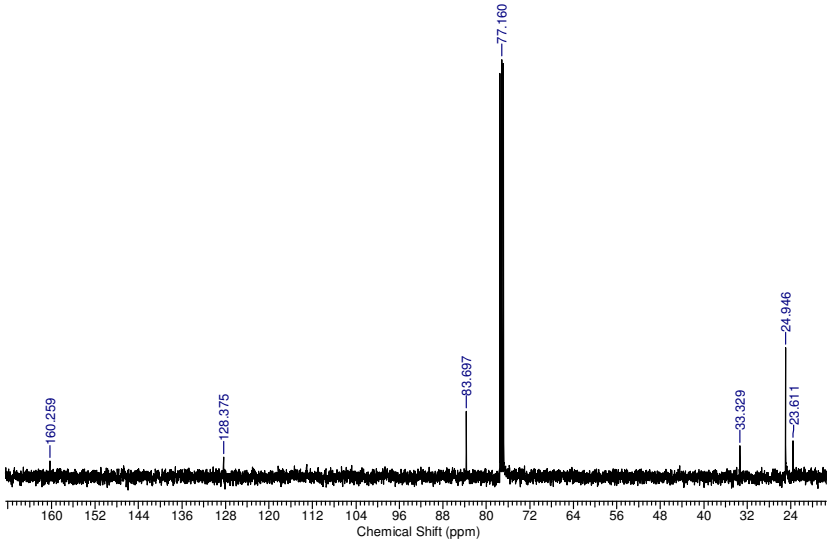

Figure S15: $^{13}C\{^{1}H\}$ NMR spectrum of the reaction mixture in $CDCl_3$ upon removal of the volatiles; spectra data is consistent with no reaction between I_2 and **B-6-Te-B**.

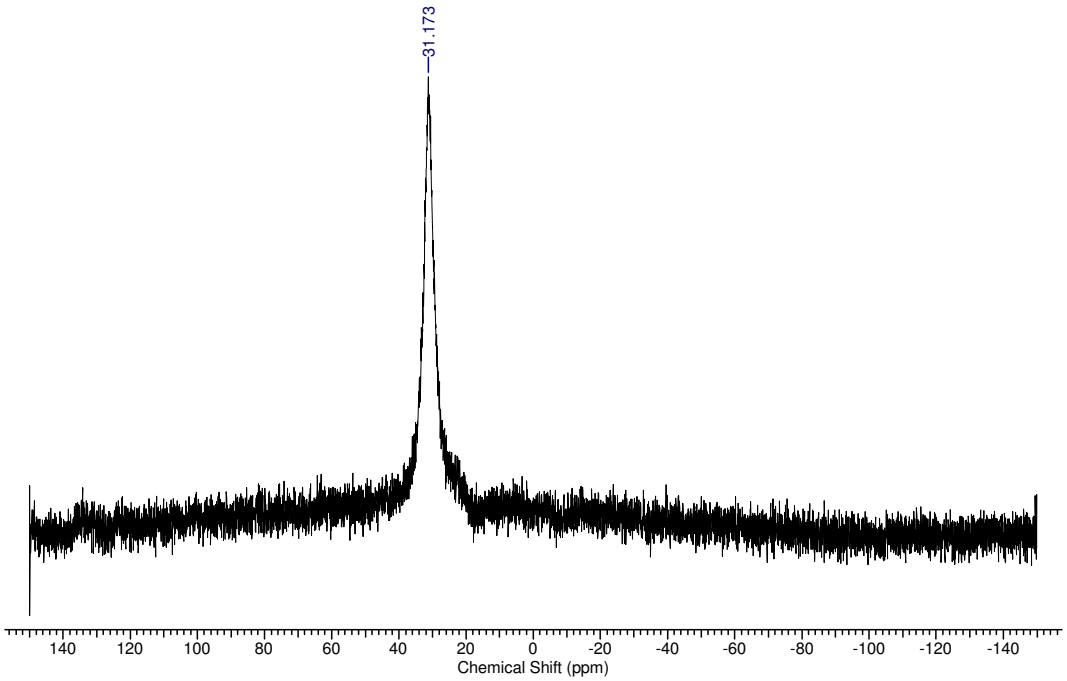

Figure S16: $^{11}B\{^{1}H\}$ NMR spectrum of the reaction mixture in $CDCl_3$ upon removal of the volatiles; spectra data is consistent with no reaction between I_2 and **B-6-Te-B**.